# Control of Radiative Processes Using Tunable Plasmonic Nanopatch Antennas

Alec Rose,[†,‡] Thang B. Hoang,[†,§] Felicia McGuire,[†,‡] Jack J. Mock,[†,‡] Cristian Ciracì,[†,‡] David R. Smith,[†,‡,§] and Maiken H. Mikkelsen*,[†,‡,§]

[†]Center for Metamaterials and Integrated Plasmonics, [‡]Department of Electrical and Computer Engineering, and [§]Department of Physics, Duke University, Durham, North Carolina 27708, United States

S Supporting Information

ABSTRACT: The radiative processes associated with fluorophores and other radiating systems can be profoundly modified by their interaction with nanoplasmonic structures. Extreme electromagnetic environments can be created in plasmonic nanostructures or nanocavities, such as within the nanoscale gap region between two plasmonic nanoparticles, where the illuminating optical fields and the density of radiating modes are dramatically enhanced relative to vacuum. Unraveling the various mechanisms present in such coupled systems, and their impact on spontaneous emission and other radiative phenomena, however, requires a suitably reliable and precise means of tuning the plasmon resonance of the nanostructure while simultaneously preserving the electromagnetic characteristics of the enhancement region. Here, we achieve this control using a plasmonic platform consisting of colloidally synthesized nanocubes electromagnetically coupled to a metallic film. Each nanocube resembles a nanoscale patch antenna (or nanopatch) whose plasmon resonance can be changed independent of its local field enhancement. By varying the size of the nanopatch, we tune the plasmonic resonance by ∼200 nm, encompassing the excitation, absorption, and emission spectra corresponding to Cy5 fluorophores embedded within the gap region between nanopatch and film. By sweeping the plasmon resonance but keeping the field enhancements roughly fixed, we demonstrate fluorescence enhancements exceeding a factor of 30 000 with detector-limited enhancements of the spontaneous emission rate by a factor of 74. The experiments are supported by finite-element simulations that reveal design rules for optimized fluorescence enhancement or large Purcell factors.
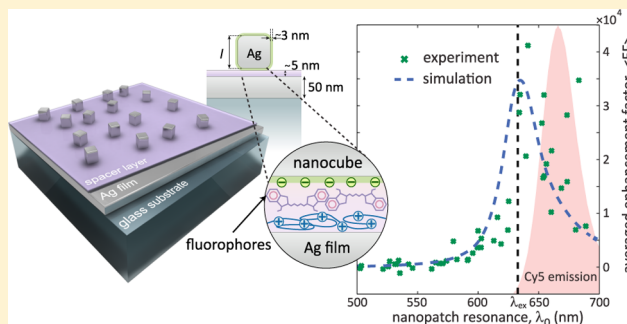
KEYWORDS: Plasmonics, plasmon resonance, nanoantennas, fluorescence enhancement, Purcell factor, nanocube, metasurface

The next generation of optical processing and sensing technologies requires significant advances in the integration of quantum emitters, such as fluorescent molecules and quantum dots, into optical platforms.[1,2] Plasmonic cavities and nanoantennas have proven to be particularly attractive candidates for modifying the excitation and decay rates of nearby emitters.[3−6] Following the pioneering work of Purcell,[7] the manipulation of spontaneous emission has found applications across a wide spectrum of modern technologies, including lasers,[8] bioimaging,[9] and modern displays.[10] In particular, emitters in close proximity to plasmonic nanostructures can have their rates of spontaneous decay increased by orders of magnitude.[11−13] The design of such systems for enhanced emission, however, is not straightforward due to the nonradiative decay channels introduced by the bare metal.[14−16] A variety of nanostructures have been shown to modify the relative radiative versus nonradiative decay rates of embedded emitters using plasmonic antennas and cavities;[3,6,17−22] for example, Kinkhabwala et al. have demonstrated single-molecule enhancement factors of 1340 from bowtie nanoantennas fabricated by electron-beam lithography.[5] However, bowtie

and closely spaced nanoparticle structures, including film-coupled spheres, have a fundamental limitation in that both field enhancement and resonance wavelength scale inversely with the gap size. Thus, previous experimental studies have been limited to broad plasmonic resonances that simultaneously overlap the emitter's excitation and emission spectra,[5] broad emitters,[6] or plasmonic cavities that are spectrally unmatched with the emitter.[20]

By hybridizing optical patch antennas with fluorophores, we demonstrate enhancement of both absorption and spontaneous emission as a function of plasmon resonance. Using this tunable platform, we achieve fluorescence enhancement factors exceeding 30 000 of fluorophores coupled to nanopatches resonating close to the excitation wavelength and spontaneous emission rates increased by at least a factor of 74. Additionally, compared to electron-beam lithography, the colloidally synthesized nanopatch (Figure 1a) is an inherently inexpensive and flexible

plasmonic platform, ideal for both large-scale and tunable applications.[23]
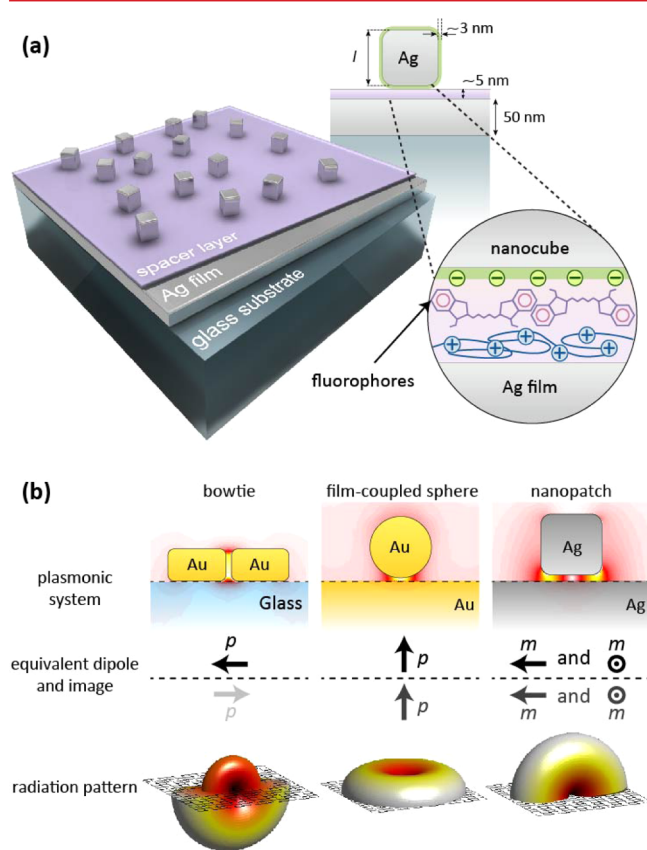
Figure 1. The plasmonic nanopatch antenna. (a) Schematic of the plasmonic nanopatch antenna platform, consisting of colloidally synthesized nanocubes dispersed over a silver film and separated by a fluorophore-coated spacer layer. (b) Comparison of typical plasmonic enhancement systems. The top row shows the geometry and resonant electric field distribution, while the bottom rows describe the plasmonic systems qualitatively through effective and image dipoles and radiation patterns. The field distributions and radiation patterns were obtained from COMSOL multiphysics simulations.

The nanopatch antennas consist of colloidally synthesized silver nanocubes deposited over a 50 nm thick silver film. The cubes and film are separated by an ∼5 nm self-assembled polyelectrolyte (PE) spacer layer, coated with a dilute layer of fluorophores (sulfo-cy5 carboxylic acid (Cy5), inset in Figure 1a). The nanopatch naturally couples to a high density of radiative modes. It is important to note that while field enhancement has been exploited for many plasmonic particles and dimers,[5,24,25] the resonance in the nanopatch is fundamentally different. Figure 1b provides a schematic comparison of the nanopatch antenna properties with two well-known systems (the bowtie antenna and the film-coupled nanoparticle). Effective dipole orientation of the plasmonic modes can be inferred from field distribution and allows for a qualitative understanding of the far-field radiation properties. The bowtie antenna and plasmonic dimer (or film-coupled sphere) can both be described as the hybridization of plasmonic resonances that exist for each isolated element into symmetric and antisymmetric resonances with the latter capable of coupling energy between the highly confined gap and free-space. In such a system, excitation and radiation tend to follow

that of an electric dipole, and spectral scaling is limited by the achievable gap sizes. As such, scaling the optical resonance of bowties and plasmonic dimers across as much as 200 nm is exceedingly difficult.[26] In the nanopatch, however, the region between the flat faces of the nanocube and the metal film introduces a gap-plasmon mode, which can propagate parallel to the film. Multiple reflections at the nanocube edges cause the gap-plasmon to undergo a Fabry–Perót-like resonance with electric field maxima at the edges, as shown in Figure 1b. These modes have two favorable properties; (i) their resonance wavelength can be controlled by varying either the nanocube size or the size of the gap; and (ii) the nanopatch couples to incident light predominantly through the magnetic field, making the coupling with external detectors significantly more efficient (see Figure 1b).

To investigate fluorescence enhancements within the nanopatch system, 48 isolated nanopatches with side-lengths ranging from 50 to 100 nm were studied. Under white-light, dark-field illumination, the nanopatches are observed as bright, diffraction-limited point scatters with colors throughout the visible spectrum corresponding to their resonance wavelength (Figure 2a). The same region is later imaged with a scanning electron microscope (SEM) enabling the size and shape of each of the 48 nanopatches to be determined in addition to their resonance wavelength. To measure the cavity mode resonance wavelength (λ_0) of individual nanopatches an image plane pinhole aperture was used and the elastic scattering of the nanopatches was dispersed by a spectrometer and detected by a charge-coupled device (CCD) camera, as shown for two typical nanopatches in Figure 2b. Subsequently, the nanopatches were excited by a continuous wave HeNe laser ($\lambda_{ex} = 632.8$ nm) and the fluorescence image (spectrally filtered by a 633 nm long pass filter) from the fluorophores was measured by another CCD camera. The fluorescence image, taken without a pinhole aperture, is then overlaid with the original color dark-field scattering image and related to the nanopatch resonance spectra. Fluorescence enhancement factors, averaged over different positions of fluorephores under a single cube, are calculated according to $\langle EF \rangle = (P_{np}/P_c)(A_{roi}/A_{np})$, where P_{np} is the fluorescence intensity collected at far-field and integrated over a region of interest containing a single nanopatch; P_c is the same quantity from a control sample consisting of glass, spacer layers, and Cy5; $A_{roi} = 8.163$ μm^2 is the region of interest defined by an area of pixels on the camera; and A_{np} is the physical cross-section of each individual nanopatch, as measured by SEM.

Even though all 48 nanopatches had a gap size of ∼8 nm, the measured fluorescence intensity ranged from near background levels to enhancements of more than 4 orders of magnitude. The fluorescence enhancement factors are shown as a function of resonance wavelength in Figure 2c. While the statistical variation in the measured enhancement factors can be attributed to the random distribution of fluorophores on the spacer layer, the enhancement factors show a strong correlation with the nanopatch resonance. In particular, the nanopatches with the largest averaged enhancement factors resonate close to the excitation wavelength, indicative of enhanced absorption in the embedded fluorophores. While the Purcell factor cannot be probed directly in the continuous wave regime, it is important to note that the sheer magnitude of fluorescence radiated by spectrally matched nanopatches implies that the fluorescence is not quenched by the proximity of the metal.
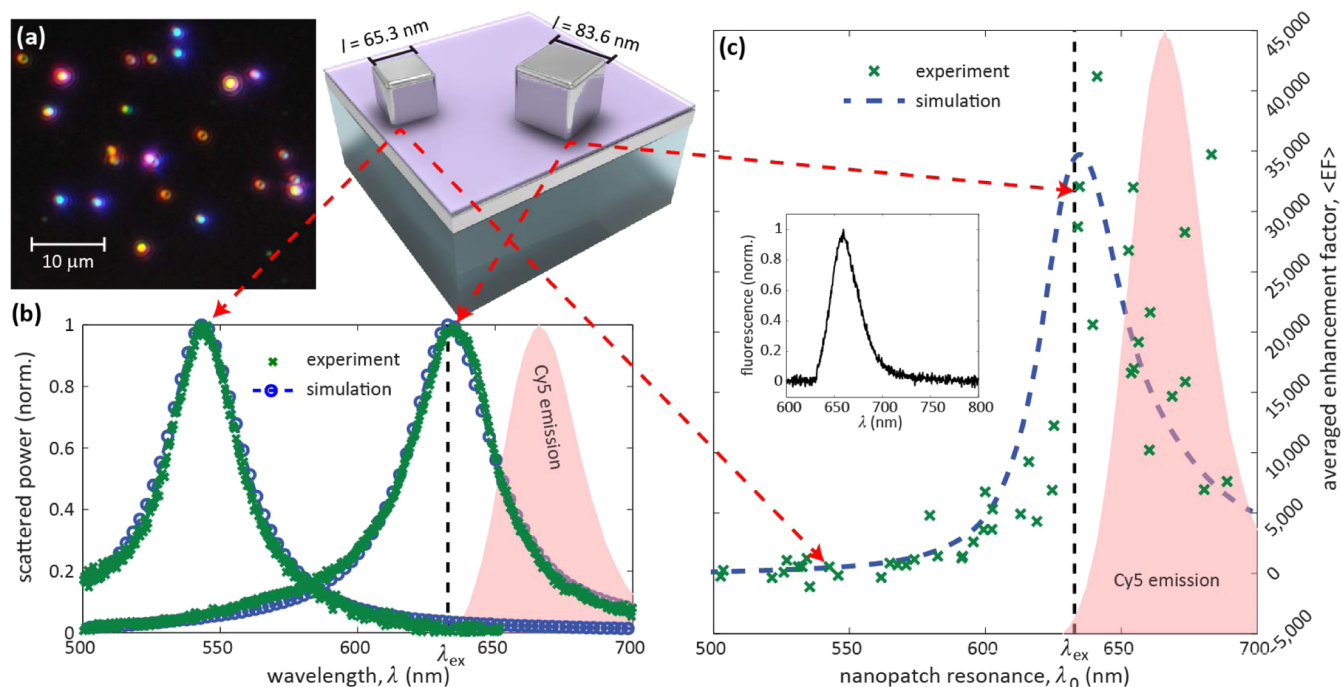
Figure 2. Nanopatch scattering and fluorescence enhancement. (a) Dark-field microscope image of the nanopatches under white-light illumination. The dominant color of each nanopatch corresponds to the resonant wavelength (λ_0) of its cavity mode. (b) Normalized scattering spectrum for two nanopatches. (c) Fluorescence enhancement factor for individual nanopatches as a function of nanopatch resonance. The inset shows a typical fluorescence spectrum from a nanopatch. Laser excitation (λ_{ex}, vertical line) and Cy5 in-solution emission spectra (shaded region) are shown for comparison.
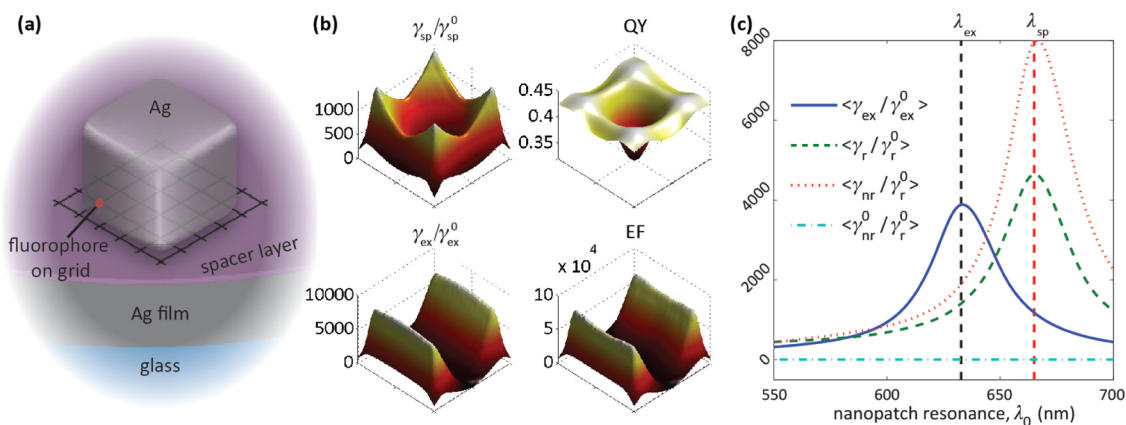

Figure 3. Nanopatch numerical model and results. (a) Schematic of the numerical model for calculating the excitation and emission from fluorophores placed in the gap of the nanopatch antenna. (b) Simulated emission properties of the excitation-correlated nanopatch as a function of fluorophore position. (c) The simulated excitation, radiative, and nonradiative rates as a function of nanopatch resonant wavelength, averaged over all locations of the fluorophore underneath the nanopatch. The internal decay rate of Cy5, $\gamma_{nr}^0 \approx 4\gamma_r^0$, is shown to be negligible by comparison.

To elucidate the intermediate steps in the observed fluorescence enhancement, and further differentiate the absorption enhancement and Purcell factor in the nanopatch system, we turn to finite-element simulations. From a theoretical perspective, we can approximate the fluorophore as a quasi-two level emitter in a complex environment. For weak optical excitation (no saturation) by a laser with wavelength λ_{ex}, the rate of excitation is given by[3]

$$\frac{\gamma_{ex}}{\gamma_{ex}^0} = \frac{|\vec{E}_{ex} \cdot \vec{n}_p|^2}{|\vec{E}_{ex}^0 \cdot \vec{n}_p|^2} \qquad (1)$$

where $\vec{n}_p$ is the orientation unit-vector of the emitter, $\vec{E}_{ex}$ is the local exciting electric field, and the superscript "0" denotes the value for the control sample. The total rate of spontaneous decay is given by $\gamma_{sp} = \gamma_r + \gamma_{nr}$, where γ_r and γ_{nr} are, respectively, the rates of radiative decay and nonradiative decay in which the latter includes the generation of surface and localized modes and thermal dissipation in the environment, among other nonradiative processes.[14−16] The Purcell factor is the total decay rate enhancement, $\gamma_{sp}/\gamma_{sp}^0$. In a lossy environment, however, it is of practical importance to know how many photons are emitted in a radiative state (rather than nonradiative), thus it is more convenient to consider the radiative decay rate enhancement γ_r/γ_r^0.[27] At steady state, the
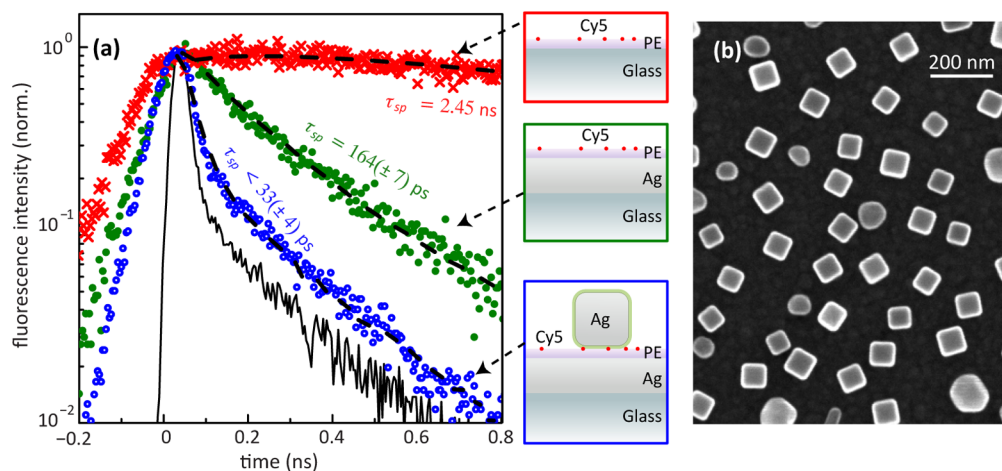
Figure 4. Fluorescence lifetime measurements. (a) Time-dependent fluorescence intensity from Cy5 embedded in nanopatches (blue), and on glass (red), and silver (green) control samples. The black line shows the measured IRF. Dashed lines are fits deconvolved with the IRF. (b) SEM image of the high density coverage ($\sim$5%) of nanopatches used for the lifetime measurements.

important parameter from an emission perspective is the probability that relaxation will yield a radiated photon, given by the quantum yield

$$QY = \frac{\gamma_r}{\gamma_{sp}} \tag{2}$$

While a large radiative enhancement is not directly responsible for large fluorescence enhancement, it is necessary to avoid quenching by the large nonradiative rates in typical plasmonic systems. Finally, in any given experiment we must also include a factor, η, that represents the probability that an emitted photon will reach the detector, that is, the collection efficiency. The total fluorescence enhancement factor is then given by

$$EF = \frac{\eta \gamma_{ex} QY}{\eta^0 \gamma_{ex}^0 QY^0} \tag{3}$$

where η is the collection efficiency, γ_{ex} is the excitation rate, QY is the quantum yield, and the superscript "0" denotes the corresponding values for the control sample.

Using finite-element simulations to probe eq 3 (COMSOL multiphysics), we demonstrate qualitative agreement in both trend and magnitude with the measured enhancement factors as a function of nanopatch resonance (dashed blue line in Figure 2c). The resonances and excitation enhancement of the individual nanopatches were obtained in a manner similar to ref 23, using a spherical domain with absorbing boundaries to model the scattering from a nanocube over a silver film. To account for additional losses in the silver film due both to surface roughness and the formation of oxide layers, we increased the imaginary part of the permittivity by a factor of 1.75 to match the simulated full width at half-maxima in the elastic scattering to that obtained in experiment (Figure 2b). To calculate the emissive properties, additional simulations were performed following the procedure outlined in ref 3 (see Supporting Information), modeling the Cy5 molecules as monochromatic point-dipoles (λ_{sp} = 665 nm) located all along a grid in the gap between the nanocube and the spacer layer (Figure 3a). The various rates for the excitation-matched nanopatch (l = 83.6 nm) are shown as a function of position in the gap (Figure 3b). The local electric fields in the nanopatch are up to 2 orders of magnitude larger than the incident fields,

such that the largest single-molecule enhancement factors occur in fluorophores located at the corners and edges. The high spatial variation in the various properties can potentially explain the variance found in the measured data of Figure 2c, because even small differences in the location and density of fluorophores under two identical cubes could drastically affect the observable quantities. Finally, assuming that the fluorophores are randomly distributed over the surface, the fluorescence enhancement factors were averaged over all orientations and locations under the cube and normalized by the same quantities obtained from simulations of the control sample.

The average simulated excitation, radiative, and nonradiative rates are shown in Figure 3c as a function of nanopatch resonance. In a lossless environment, γ_{nr}, and thus the quantum yield, is determined by internal channels of decay. Extrapolating the internal decay rate of Cy5 from its in-solution quantum yield ($\sim$20%), however, it becomes clear that the internal decay channel is simply too slow to significantly contribute in the proximity of the plasmonic resonance.[5] Instead, spontaneous decay in the nanopatch can be visualized as a two-step process. First, via the Purcell effect the excited fluorophore experiences an enhanced decay rate into one of the gap-plasmon modes of the nanopatch. From here, the gap-plasmons couple to radiative modes, are absorbed within the metal, or couple to surface modes. This second step is defined by the nanopatch geometry and is key in avoiding quenching. By comparison, fluorophores sufficiently close to a bare silver film experience increased decay rates into surface-plasmon modes, enhancing the spontaneous decay rate at resonance.[28] In the absence of nanostructures and defects, however, these surface modes do not radiate and contribute only to the nonradiative rate. This difference in the nanopatch, namely the subsequent coupling of gap-plasmons to radiative modes, explains why the quantum yield is not quenched, but instead stays in the range of 35−45%. This persists even in nanopatches resonating at the Cy5 peak emission, reaching theoretical average radiative decay enhancement of more than 4000. On the other hand, the largest field localization occurs at the nanopatch resonance, such that the rate of excitation, and thus $\langle EF \rangle$, is markedly enhanced for nanopatches resonating at λ_{ex}. Finally, the simple directivity of the magnetically coupled nanopatch increases collection

efficiency by roughly 1 order of magnitude when compared to a bare glass film. Taken together, these factors account for the giant enhancements of ∼30 000 in the measured fluorescence from nanopatches matched near the laser excitation wavelength.

We also probe the Purcell effect directly by measuring the spontaneous decay lifetimes (τ_{sp}). For these measurements, the fluorophores were excited using an 80 MHz Ti:sapphire laser with a frequency-doubled OPO output at 632 nm and detected using a fast timing avalanche photodiode (PDM, Micro Photon Device) and a time-correlated single-photon counting module (PicoHarp 300, Picoquant). The fluorescence lifetimes were measured from an ∼20 μm diameter surface area covered by a higher density (∼5%) of uniform nanopatches ($\lambda_0 \sim \lambda_{ex}$, Figure 4b) and a lower density of fluorophores (1/25× original) as shown in Figure 4a. The measurement was repeated for a control sample consisting of glass, spacer layer, and Cy5, as well as another control sample consisting of silver film, spacer layer, and Cy5; both were without silver nanocubes. Lifetimes were obtained from fits to the data deconvolved with the instrument response function (IRF).[29] Compared to the control sample on glass ($\tau_{sp}^0 = 2.54 \pm 0.04$ ns) we observed a significant shortening of the Cy5 lifetimes when deposited over the silver film ($\tau_{sp} = 164 \pm 7$ ps). For Cy5 fluorophores on the nanopatch sample, a biexponential decay is observed with a fast decay component of $\tau_{sp} = 33 \pm 4$ ps due to fluorophores coupled to the nanopatches, and a slower decay component of $\tau_{sp} = 157 \pm 5$ ps attributed to uncoupled fluorophores on the silver film. The measured lifetimes of fluorophores coupled to nanopatches is close to the detector's IRF, thus providing only an upperbound on the lifetime. While such measurements could be improved upon,[30] even so we observe a 74-fold reduction in the fluorescence lifetime compared to the control sample on glass, demonstrating that the plasmonic-enhanced fluorescence in the nanopatch system is indeed accompanied by a significant enhancement in the spontaneous emission rate. While the Cy5 over the silver film also exhibited a shortened lifetime, it is important to note that the emission intensity was disproportionately weaker compared with the nanopatch sample, as expected from the quenching effect of metal films. To verify this, we measured the emission intensity from Cy5 fluorophores distributed over silver films with different thickness polyelectrolyte layers (see Supporting Information). As an illustrative example, for a layer thickness of 5 nm the fluorescence intensity was reduced by a factor of 20 compared with the glass slide, which is in complete contrast to the orders of magnitude enhancement when the nanopatches are included. Thus, by optimizing nanopatches to resonate at either a fluorophore's peak emission or excitation wavelength, this flexible platform can alternately optimize the Purcell or fluorescence enhancement factors.

While the fluorescence enhancement experiments purposefully used a nonuniform population of nanopatches, a surface of uniform and properly tuned nanopatch antennas can function as an ideal, large-area emitter. Also, the nanopatch platform is promising for biosensing and fluorescence imaging applications[9,31] with the potential to enhance the performance of conventionally poor labels. Owing to the flexibility and excellent scaling properties of the colloidally synthesized nanopatches, it is likely that future studies will reveal even better geometries and materials, further paving the way toward inexpensive single-photon sources for quantum information applications.[1]

Methods. The samples were fabricated by evaporation of Ag/Ge (50 nm/4 nm) films on glass slides followed by deposition of five layers of alternating poly(allylamine) hydrochloride (PAH) and polystyrenesulfonate (PSS). From ellipsometry measurements, the total thickness of these polyelectrolyte layers was found to be 5.0 ± 0.1 nm. Next, the samples were exposed to a 25 μM sulfo-Cy5 carboxylic acid derivative for 10 min, followed by deposition of silver nanocubes resulting in a surface coverage of ∼1%. Control samples were fabricated in a similar manner on bare glass substrates and on Ag/Ge films but without nanocubes. Silver nanocubes were chemically synthesized with minor modifications to previously published procedures,[23,32] resulting in slightly rounded cubes and coated in a polyvinylpyrrolidone (PVP) layer with an estimated thickness of 1−3 nm. Additional details are provided in the Supporting Information.

An optical dark-field microscope with an extra long working distance objective (50×, 0.55NA 8.2 mm WD) was used for both scattering, fluorescence intensity, and lifetime measurements. Nanopatches were illuminated from ∼62° off-normal incidence using a multimode fiber for scattering measurements and a 632.8 nm continuous wave HeNe laser for fluorescence enhancement measurements. The signal from individual nanopatchs was isolated at the image plane by a pinhole aperture and directed to a spectrometer and CCD camera for scattering and fluorescence spectrum measurements. Fluorescence from both nanopatches and control samples were spectrally filtered by a long pass filter and imaged (without a pinhole aperture) for enhancement factor measurements. The enhancement factor of each nanopatch was calculated by comparing the intensity of the fluorescence from Cy5 fluorophores under a single nanocube with the fluorescence from an equivalent area on the glass control sample. Both numbers were corrected for background fluorescence (due to the pinhole size being larger than the size of the nanocube), camera read noise, and exposure length.

■ ASSOCIATED CONTENT

ⓢ Supporting Information
Description of the theoretical modeling, sample fabrication, and experimental procedures. This material is available free of charge via the Internet at http://pubs.acs.org.

■ AUTHOR INFORMATION

Corresponding Author
*E-mail: m.mikkelsen@duke.edu.

Present Address
(C.C.) Istituto Italiano di Tecnologia (IIT), Center for Biomolecular Nanotechnologies, Via Barsanti, I-73010 Arnesano, Italy.

Notes
The authors declare no competing financial interest.

■ REFERENCES

(1) Kimble, H. J. *Nature* **2008**, *453*, 1023−1030.
(2) Schietinger, S.; Barth, M.; Aichele, T.; Benson, O. *Nano Lett.* **2009**, *9*, 1694−1698.

(3) Anger, P.; Bharadwaj, P.; Novotny, L. *Phys. Rev. Lett.* **2006**, *96*, 113002.

(4) Tam, F.; Goodrich, G. P.; Johnson, B. R.; Halas, N. J. *Nano Lett.* **2007**, *7*, 496−501.

(5) Kinkhabwala, A.; Yu, Z.; Fan, S.; Avlasevich, Y.; Mllen, K.; Moerner, W. E. *Nat. Photonics* **2009**, *3*, 654−657.

(6) Russell, K. J.; Liu, T.-L.; Cui, S.; Hu, E. L. *Nat. Photonics* **2012**, *6*, 459−462.

(7) Purcell, E. M.; Torrey, H. C.; Pound, R. V. *Phys. Rev.* **1946**, *69*, 37−38.

(8) Yablonovitch, E. *Phys. Rev. Lett.* **1987**, *58*, 2059−2062.

(9) Lakowicz, J. R. *Anal. Biochem.* **2001**, *298*, 1−24.

(10) Friend, R. H.; Gymer, R. W.; Holmes, A. B.; Burroughes, J. H.; Marks, R. N.; Taliani, C.; Bradley, D. D. C.; Santos, D. A. D.; Brédas, J. L.; Lögdlund, M.; Salaneck, W. R. *Nature* **1999**, *397*, 121−128.

(11) Drexhage, K. *J. Lumin.* **1970**, *12*, 693−701.

(12) Geddes, C. D.; Lakowicz, J. R. *J. Fluoresc.* **2002**, *12*, 121−129.

(13) Lakowicz, J. R. *Anal. Biochem.* **2005**, *337*, 171−194.

(14) Morawitz, H. *Phys. Rev.* **1969**, *187*, 1792−1796.

(15) Chance, R. R.; Prock, A.; Silbey, R. *J. Chem. Phys.* **1974**, *60*, 2744−2748.

(16) Becker, H.; Burns, S. E.; Friend, R. H. *Phys. Rev. B* **1997**, *56*, 1893−1905.

(17) Kühn, S.; Håkanson, U.; Rogobete, L.; Sandoghdar, V. *Phys. Rev. Lett.* **2006**, *97*, 017402.

(18) Fort, E.; Grésillon, S. *J. Phys. D: Appl. Phys.* **2008**, *41*, 013001.

(19) Bakker, R. M.; Drachev, V. P.; Liu, Z.; Yuan, H.-K.; Pedersen, R. H.; Boltasseva, A.; Chen, J.; Irudayaraj, J.; Kildishev, A. V.; Shalaev, V. M. *New J. Phys.* **2008**, *10*, 125022.

(20) Yi, M.; Zhang, D.; Wen, X.; Fu, Q.; Wang, P.; Lu, Y.; Ming, H. *Plasmonics* **2011**, *6*, 213−217.

(21) Szmacinski, H.; Badugu, R.; Mahdavi, F.; Blair, S.; Lakowicz, J. R. *J. Phys. Chem. C* **2012**, *116*, 21563−21571.

(22) Frimmer, M.; Koenderink, A. F. *Phys. Rev. Lett.* **2013**, *110*, 217405.

(23) Moreau, A.; Ciracì, C.; Mock, J. J.; Hill, R. T.; Wang, Q.; Wiley, B. J.; Chilkoti, A.; Smith, D. R. *Nature* **2012**, *492*, 86−89.

(24) Zhang, J.; Fu, Y.; Chowdhury, M. H.; Lakowicz, J. R. *Nano Lett.* **2007**, *7*, 2101−2107.

(25) Sorger, V. J.; Pholchai, N.; Cubukcu, E.; Oulton, R. F.; Kolchin, P.; Borschel, C.; Gnauck, M.; Ronning, C.; Zhang, X. *Nano Lett.* **2011**, *11*, 4907−4911.

(26) Zhu, W.; Banaee, M. G.; Wang, D.; Chu, Y.; Crozier, K. B. *Small* **2011**, *7*, 1761−1766.

(27) Sauvan, C.; Hugonin, J. P.; Maksymov, I. S.; Lalanne, P. *Phys. Rev. Lett.* **2013**, *110*, 237401.

(28) Chance, R. R.; Prock, A.; Silbey, R. *J. Chem. Phys.* **1975**, *62*, 2245−2253.

(29) Enderlein, J.; Erdmann, R. *Opt. Commun.* **1997**, *134*, 371−378.

(30) Cho, C.-H.; Aspetti, C. O.; Turk, M. E.; Kikkawa, J. M.; Nam, S.-W.; Agarwal, R. *Nat. Mater.* **2011**, *10*, 669−675.

(31) Schultz, S.; Smith, D. R.; Mock, J. J.; Schultz, D. A. *Proc. Natl. Acad. Sci. U.S.A.* **2000**, *97*, 996−1001.

(32) Zhang, Q.; Li, W.; Wen, L.-P.; Chen, J.; Xia, Y. *Chem.—Eur. J.* **2010**, *16*, 10234−10239.